Analysis of the ambiguity in the determination of quantum yields from spectral data on a photoinduced isomerization

Henning Schröder[a,b,*], Cyril Ruckebusch[c], Olivier Devos[c], Rémi Métivier[d], Mathias Sawall[a], Denise Meinhardt[a,b], Klaus Neymeyr[a,b]

[a] *Universität Rostock, Institut für Mathematik, 18057 Rostock, Germany*
[b] *Leibniz-Institut für Katalyse, 18059 Rostock, Germany*
[c] *Univ. Lille, CNRS, UMR 8516 - LASIR - Laboratoire de Spectrochimie infrarouge et Raman, 59000 Lille, France*
[d] *ENS Cachan, CNRS, UMR 8531 - PPSM - Laboratoire de Photophysique et Photochimie Supramoléculaires et Macromoléculaires, 94235 Cachan Cedex, France*

Abstract

Multivariate curve resolution (MCR) helps to uncover the spectra and concentration profiles of the pure components from sequences of spectra measured at a chemical reaction system. However, the underlying matrix factorization problem has often multiple solutions. This fact is known under the keyword rotational ambiguity and explains why different MCR methods can provide different decompositions for the same data. Kinetic reaction models can be used in order to constrain the feasible concentration profiles. This reduces the rotational ambiguity. Especially in the case that a first-order reaction model is assumed, the remaining ambiguity can be described completely analytically.

A hard-model based MCR method is used for the simultaneous analysis of multiple data sets. The method is tested for a reversible two-step photokinetic model. The kinetic model cannot enforce a single, unique solution. Instead the remaining ambiguity is fully investigated. The practical benefit of the method is demonstrated for an experimental UV/Vis data set of a photoinduced isomerization.

Keywords: Multivariate curve resolution, Kinetic modeling, Ambiguity of kinetic parameters, Multiset analysis.

1. Introduction

Multivariate curve resolution (MCR) techniques are highly useful for the analysis of chemical reaction systems. Their central objective is the reliable extraction of pure component information from time series of spectra. Let $D \in \mathbb{R}^{m\times n}$ be the row-wise matrix representation of a sequence of m spectra, each with n data channels. For an s-component chemical reaction system the aim is to determine nonnegative factors $C \in \mathbb{R}^{m\times s}$ and $S \in \mathbb{R}^{n\times s}$ so that

$$D = CS^T \tag{1}$$

holds. Any pair of nonnegative matrices C and S that fulfills Equation (1) is called *feasible*. The occurrence of multiple nonnegative matrix pairs (C, S) satisfying (1) is paraphrased by the keyword *rotational ambiguity* [1, 2, 3]. An important challenge of MCR analyses is to identify those feasible factors that contain chemically meaningful information. A number of different approaches has been proposed in the literature to overcome this problem. On one hand there are optimization-based MCR methods which in combination with additional constraints yield by their construction a single pair of feasible factors. This solution is often assumed to be the true, chemically correct solution [4, 5, 6]. On the other hand there are global methods which yield the set of all feasible factorizations of D. A prominent global method is the feasible bands approach [7] that represents all feasible matrix factors in plots of the bands of all feasible spectra and concentration profiles. An alternative global approach is the *Area of feasible solutions* (AFS) representation [8, 9, 10, 11], which provides a low-dimensional representation of the feasible bands in terms of the expansion coefficients of the left and right singular vectors of D.

*Corresponding author

Kinetic reaction models can be combined with each of these techniques [2, 12, 13]. A kinetic model helps to restrict the set of feasible concentration profiles to those curves that are possible solutions of the kinetic reaction equations for optimized kinetic parameters. In general, kinetic models are well-known to be very effective in reducing the rotational ambiguity [12, 14, 15]. However, the usage of consecutive first-order reaction models is often not sufficient in order to obtain a unique solution [16, 17, 18]. See also [19] for a general approach to this problem with arbitrary first-order models. In this work, the methodology is to consider the set of all feasible factors C and S for which a given kinetic model can be parameterized in a way that the concentration profiles are consistent with the factor C. An elegant and concise representations of these consistent factors is possible by collecting all the associated kinetic parameters within a set of D-consistent parameters $\mathcal{K}$, see [19]. This representation enables an unbiased analysis of the feasible factorizations under the constraint of a kinetic model and reveals the underlying correlations of the kinetic parameters.

In this paper the set of D-consistent parameters (here in the form of quantum yields) $\mathcal{K}$ is derived for the reversible two-step photokinetic model $Y \leftrightarrow X \leftrightarrow Z$. Therefore a hard-modeling approach is introduced which can be applied to multisets [20, 21, 22]. This enables the calculation of a pair of feasible factors, which determine an initial element in the set $\mathcal{K}$. Based on this initial element, equations for the analytical description of the set $\mathcal{K}$ are derived. This makes it possible to evaluate the rotational ambiguity under the constraint of the given photokinetic model.

1.1. Organization of the paper

Section 2 presents a kinetic hard-modeling approach for multisets. The reversible two-step photokinetic model is analyzed in Section 3. To this end, the model is introduced, the analytical derivation of the set of D-consistent quantum yields is derived in Section 3.1 and an approximation of the photokinetic factor is presented in Section 3.2. Finally, the results are applied to an UV/Vis multiset in Section 4.

2. Kinetic hard-modeling for multisets

The "classical" MCR analysis of an s-component system involves the extraction of concentration profiles and spectra of the pure components from a sequence of m spectra stored in a matrix $D \in \mathbb{R}^{m\times n}$. Nonnegative factors $C \in \mathbb{R}^{m\times s}$ and $S \in \mathbb{R}^{n\times s}$ are to be determined such that (1) holds (at least approximately). The intrinsic ambiguity of this problem often requires the usage of a-priori assumptions on the factors C and/or S, e.g. kinetic models, unimodality, monotonicity or selectivity [14]. This ambiguity can also be reduced by analyzing multiple, differing data sets of the same reaction system. Such data can be acquired by a repeated execution and measurement of the experiment under different conditions. The resulting collection of data sets can be concatenated into a so-called multiset. The higher-dimensional multiset data can be processed in a simultaneous analysis. In this section we present a modification of the kinetic hard-modeling approach from [19], which can be applied to multisets that are regularized by photokinetic models. Our approach is based on ideas from [12]. If the reader is familiar with the analysis of multisets and hard-model approaches, then the remaining part of this section can be skipped.

A common experimental setup is to vary one or several properties of a reaction system (e.g. initial concentrations, pressure, pH-value, etc.) and to measure time-dependent series of spectra under the changed conditions. This results in p data sets $D_1 \in \mathbb{R}^{m_1\times n}, \ldots, D_p \in \mathbb{R}^{m_p\times n}$ with $m_i, i = 1, \ldots, p$, being the numbers of time points of the i-th data set and n the number of data channels of every spectrum. The underlying assumption is that only the dynamic behavior of the species is different between the individual data sets, whereas their spectra remain unchanged. The p matrices D_i are concatenated to form the matrix

$$D = \begin{pmatrix} D_1 \\ \vdots \\ D_p \end{pmatrix} \in \mathbb{R}^{m_t\times n} \tag{2}$$

with $m_t = m_1 + \ldots + m_p$. Under the given assumption one wants to extract a common pure spectra matrix $S \in \mathbb{R}^{s\times n}$, which fits to all $D_i, i = 1, \ldots, p$, in the sense that individual factors of concentration profiles $C_i \in \mathbb{R}^{m_i\times s}, i = 1, \ldots, p$

exits with

$$\underbrace{\begin{pmatrix} D_1 \\ \vdots \\ D_p \end{pmatrix}}_{D} = \underbrace{\begin{pmatrix} C_1 \\ \vdots \\ C_p \end{pmatrix}}_{C} S^T.$$

Next we assume that kinetic models are known for the p data sets of the investigated reaction system. The hard-modeling approach in [19, 12] is based on the minimization of an objective function $f(\phi)$ with the parameters of the kinetic model $\phi \in \mathbb{R}^q$. This hard-modeling approach has been introduced for applications to single data sets. In the following we introduce a generalization for applications to multiple bilinear data sets. Only minor changes of $f(\phi)$ are required, which are described in detail next.

In this paper we consider the case of a photokinetic model to describe the behavior of a photoreaction in which the so-called *quantum yields* take the place of the kinetic parameters in thermal reactions [27]. The p photokinetic models for the data sets $D_1, \ldots, D_p$ are defined by p initial value problems (IVP) for ordinary differential equations (ODE). Each IVP has an associated vector of initial concentrations $c_{0,i}$, $i = 1, \ldots, p$. All ODE systems depend on the (same) unknown vector of quantum yields ϕ for which optimal values are to be determined. The matrices $C_i^{\text{ode}}(\phi) \in \mathbb{R}_+^{m_i \times s}$, $i = 1, \ldots, p$, can be obtained by numerical integration of the p IVPs with respect to the given time grid. Thus these matrices represent the evaluations of the p photokinetic models. The concatenated matrix $C^{\text{ode}}(\phi) \in \mathbb{R}_+^{m_t \times s}$ is defined by

$$C^{\text{ode}}(\phi) = \begin{pmatrix} C_1^{\text{ode}}(\phi) \\ \vdots \\ C_p^{\text{ode}}(\phi) \end{pmatrix}.$$

Further let $U\Sigma V^T$ be the truncated singular value decomposition [23] of D which includes only the first s singular values and the first s left and right singular vectors. The recipe for the numerical evaluation of the target function can be taken over directly from [19]. The main computation steps are as follows:

1. Compute $C^{\text{ode}}(\phi)$ for the current quantum yields ϕ,
2. form the transformation $T = (C^{\text{ode}}(\phi))^+ U\Sigma$,
3. compute from T the associated factors $C = U\Sigma T^{-1}$ and $S^T = TV^T$ and finally
4. evaluate the function value of the objective function

$$f(\phi) = \underbrace{\sum_{i=1}^{m_t} \sum_{j=1}^{s} \min\left(\frac{C_{ij}}{\max_l(C_{lj})}, 0\right)^2}_{\text{nonnegativity constraint on } C} + \underbrace{\sum_{i=1}^{n} \sum_{j=1}^{s} \min\left(\frac{S_{ij}}{\max_l(S_{lj})}, 0\right)^2}_{\text{nonnegativity constraint on } S} + \underbrace{\|C^{\text{ode}}(\phi) - C\|_F^2}_{\text{kinetic fit}}. \tag{3}$$

Minimization algorithms as the Nelder-Mead simplex method [24] or the trust-region reflective method [25] can be used to solve the minimization problem

$$\|f(\phi)\|_2 \;\to\; \min. \tag{4}$$

This procedure yields the feasible factors C^* and S^* as well as an optimized vector of quantum yields ϕ^* of the photokinetic models.

3. Ambiguity of the photokinetic parameters

This section introduces a reversible two-step kinetic model for a photoinduced reaction system. Further the set of D-consistent quantum yields is derived for this model. The photokinetic model for the $s = 3$ components X, Y and Z reads

$$Y \underset{\phi_1}{\overset{\phi_{-1}}{\rightleftharpoons}} X \underset{\phi_{-2}}{\overset{\phi_2}{\rightleftharpoons}} Z \tag{5}$$

with the unknown vector of quantum yields $\phi = (\phi_1, \phi_{-1}, \phi_2, \phi_{-2})^T \in (0,1]^4$. The corresponding ODE system reads

$$\begin{pmatrix} \dot{x}(t) \\ \dot{y}(t) \\ \dot{z}(t) \end{pmatrix} = F(t) \cdot I \cdot M(\phi) \begin{pmatrix} x(t) \\ y(t) \\ z(t) \end{pmatrix} \tag{6}$$

with the coefficient matrix

$$M(\phi) = \begin{pmatrix} -\phi_1 - \phi_2 & \phi_{-1} & \phi_{-2} \\ \phi_1 & -\phi_{-1} & 0 \\ \phi_2 & 0 & -\phi_{-2} \end{pmatrix} \begin{pmatrix} \varepsilon_X & 0 & 0 \\ 0 & \varepsilon_Y & 0 \\ 0 & 0 & \varepsilon_Z \end{pmatrix} \tag{7}$$

and concentration profiles $x(t), y(t)$ and $z(t)$ of the three chemical species X, Y and Z. The incident monochromatic photon flux is denoted by $I \in \mathbb{R}$, the molar absorption coefficients are $\varepsilon_X, \varepsilon_Y, \varepsilon_Z \in \mathbb{R}_+$ and $F(t)$ is the time-dependent photokinetic factor.

3.1. Set of D-consistent quantum yields

The set of D-consistent parameters $\mathcal{K}$ is introduced in [19]. In brief words these are the kinetic parameter vectors whose associated ODE solutions form a factor C so that $D = CS^T$ holds for a (not necessarily nonnegative) matrix S. Therefore the determination of the set $\mathcal{K}$ is not necessarily associated with an MCR factorization problem for D, but arises for any fitting of a kinetic model to a single-wavelength measurement. In the context of photokinetic reaction systems we use the conceptual extension of a set $\mathcal{K}$ of *D-consistent quantum yields*. Analogously, for each vector of quantum yields $\phi \in \mathcal{K}$, the matrix D can be decomposed into CS^T wherein C is close to the ODE solution $C^{\text{ode}}(\phi)$ for the given vector ϕ. Thus for a given $\phi \in \mathcal{K}$ the factors C and S (should at least approximately) fulfill the equations

$$\frac{\|D - CS^T\|_F}{\|D\|_F} = 0, \quad \frac{\|C - C^{\text{ode}}(\phi)\|_F}{\|C\|_F} = 0 \quad \text{and} \quad \frac{\|\min(C,0)\|_F}{\|C\|_F} = 0.$$

The last equation guarantees the nonnegativity of C. This equation can be ignored because nonnegativity is already been guaranteed by the second equation that guarantees that C reproduces the (necessarily) nonnegative ODE solution $C^{\text{ode}}(\phi)$. All these error measure are considered in the approximate, numerical setup that is presented in Section 4. The set of feasible quantum yields $\mathcal{K}_+$ is a subset of $\mathcal{K}$ for which additionally the matrix S satisfies

$$\frac{\|\min(S,0)\|_F}{\|S\|_F} = 0.$$

The latter condition is necessary for interpreting the columns of S as the spectra of the pure components.

Next we present a closed-form expression (analytic representation) of the set $\mathcal{K}$ for the reaction system (5) with the coefficient matrix $M(\phi)$ from (7). Let a certain $\phi^* \in \mathcal{K}$ be known. Such an initial vector of quantum yields can easily be computed by the approach presented in Section 2 or any multivariate curve result method which includes kinetic model modeling. According to the main theoretical result in [19] a vector of quantum yields ϕ is in the set $\mathcal{K}$ if and only if all eigenvalues of $M(\phi)$ coincide with those of $M(\phi^*)$. The eigenvalues of $M(\phi^*)$ are

$$\begin{aligned} \lambda_1 &= 0, \\ \lambda_{2,3} &= -\frac{\kappa(\phi^*)}{2} \pm \frac{1}{2}\sqrt{\kappa(\phi^*)^2 - 4\delta(\phi^*)} \end{aligned} \tag{8}$$

with

$$\begin{aligned} \kappa(\phi^*) &= \varepsilon_X\phi_1^* + \varepsilon_Y\phi_{-1}^* + \varepsilon_X\phi_2^* + \varepsilon_Z\phi_{-2}^*, \\ \delta(\phi^*) &= \varepsilon_X\phi_1^*\varepsilon_Z\phi_{-2}^* + \varepsilon_Y\phi_{-1}^*\varepsilon_X\phi_2^* + \varepsilon_Y\phi_{-1}^*\varepsilon_Z\phi_{-2}^*. \end{aligned} \tag{9}$$

For the analytical representation of the set $\mathcal{K}$, all ϕ have to be determined which leave the eigenvalues λ_1, λ_2 and λ_3 unchanged. The set $\mathcal{K}$ contains all quantum yields $\phi \in (0,1]^4$ which meet the following conditions (see Appendix

Appendix A for details):

$$-\lambda_2 \leq \varepsilon_X\phi_2 + \varepsilon_Z\phi_{-2} \leq -\lambda_3 \tag{10}$$

$$\phi_2 > -\frac{1}{\varepsilon_X\varepsilon_Z\phi_{-2}}(\varepsilon_Z\phi_{-2} + \lambda_2)(\varepsilon_Z\phi_{-2} + \lambda_3) \tag{11}$$

$$\phi_1(\phi_2, \phi_{-2}) = -\frac{1}{\varepsilon_X^2\phi_2} \cdot (\varepsilon_X\phi_2 + \varepsilon_Z\phi_{-2} + \lambda_2) \cdot (\varepsilon_X\phi_2 + \varepsilon_Z\phi_{-2} + \lambda_3) \tag{12}$$

$$\phi_{-1}(\phi_2, \phi_{-2}) = \frac{1}{\varepsilon_Y}(\kappa(\phi^*) - \varepsilon_X\phi_1(\varepsilon_X\phi_2, \varepsilon_Z\phi_{-2}) - \varepsilon_X\phi_2 - \varepsilon_Z\phi_{-2}) \tag{13}$$

Equations (12) and (13) are explicit representations of the quantum yields ϕ_1 and ϕ_{-1} in dependence of ϕ_2 and ϕ_{-2}. Together with the bounds (10) and (11) these are two explicit representations of the set of feasible quantum yields $\mathcal{K}$. Eqns. (11)–(13) are the basis for an efficient calculation and generation of plots of the set of feasible quantum yields $\mathcal{K}$.

Remark 3.1. *Two correlations between the results of this section and other (photo-)kinetic models are:*

a) The kinetic model (5) *and the analytic representation of the set $\mathcal{K}$ can be reduced to a "classical" reversible two-step reaction by setting $F(t) = 1$ for all times t and $I = \varepsilon_X = \varepsilon_Y = \varepsilon_Z = 1$.*

b) By setting the corresponding ϕ_i values to zero, the sets $\mathcal{K}$ can be derived for various models based on the Eq. (10)-(13)*, e.g.*

$$Y \xrightarrow{\phi_{-1}} X \xrightarrow{\phi_2} Z\,, \quad Y \underset{\phi_1}{\overset{\phi_{-1}}{\rightleftharpoons}} X \xrightarrow{\phi_2} Z \quad \textit{and} \quad Y \xrightarrow{\phi_{-1}} X \underset{\phi_{-2}}{\overset{\phi_2}{\rightleftharpoons}} Z.$$

Relabelling of the components and quantum yields/rate constants might be necessary to meet common notation standards. See [19] for more details on the three models above.

3.2. Approximation of the photokinetic factor

The function $F(t)$ in (6) is not known in advance and must therefore be approximated. Photoinduced reactions are triggered by light at a chosen irradiation wavelength λ (405 nm here). If we denote by $d_\lambda(t)$ the absorption of the reaction system at the wavelength λ along the time axis t, then the *photokinetic factor* can be approximated in a general way according to

$$F(t) \approx \bar{F}(t) = \frac{1 - 10^{-d_\lambda(t)}}{d_\lambda(t)}; \tag{14}$$

see Chapter 1, Equation (1.39), in [26]. A continuous evaluation of $\bar{F}(t)$ is needed for the numerical integration of the IVPs of Section 2. Because of the discrete structure of spectroscopic data, two minor problems arise. First, the intensity profile $d_\lambda(t)$ is usually neither known for the irradiation wavelength λ nor for continuous time points t. The column of D that corresponds to the wavelength which is nearest to λ can be used to approximate $d_\lambda(t)$ on the given time grid. Second, the values $\bar{F}(t)$ are not obtainable for arbitrary time points t within the boundaries of the time grid, but can be approximated by (linear or higher order) interpolation.

4. Numerical results

A photochromic UV/Vis study of *cis*-1,2-dicyano-1,2-bis(2,4,5-trimethyl-3-thienyl)ethene (CMTE) [22, 27] is investigated in this section. The reaction system contains $s = 3$ independent components, namely different forms of CMTE: X = open *cis* isomer, Y = closed ring form and Z = open *trans* isomer. The hard-modeling approach from Section 2 is applied and the sets $\mathcal{K}$ and $\mathcal{K}_+$ are derived. Finally, an improved solution (by means of typical error measures) is identified in $\mathcal{K}_+$.

Two UV/Vis data sets $D_1 \in \mathbb{R}^{103\times 621}$ and $D_2 \in \mathbb{R}^{146\times 621}$ with 621 data channels in each of the 103 and 146 measured spectra are considered. They are shown in Fig. 1. The vector $x \in \mathbb{R}^{621}$ contains the wavelength grid and is valid for both data sets. The two data sets differ in their initial concentrations $c_{0,1} = (5.93 \cdot 10^{-5}, 0, 0)$ mol/l and $c_{0,2} = (0, 0, 1.072 \cdot 10^{-4})$ mol/l as well as their incident monochromatic photon fluxes $I_1 = 4.8 \cdot 10^{-6}$ mol/(l·s) and $I_2 = 4.5 \cdot 10^{-6}$ mol/(l·s). Both were irradiated at the same wavelength of 405 nm and the molar absorption coefficients of the different forms at this wavelength are $\varepsilon_X = 3.1075 \cdot 10^3, \varepsilon_Y = 1.0862 \cdot 10^3, \varepsilon_Z = 2.3365 \cdot 10^3$ in l/(mol· cm).

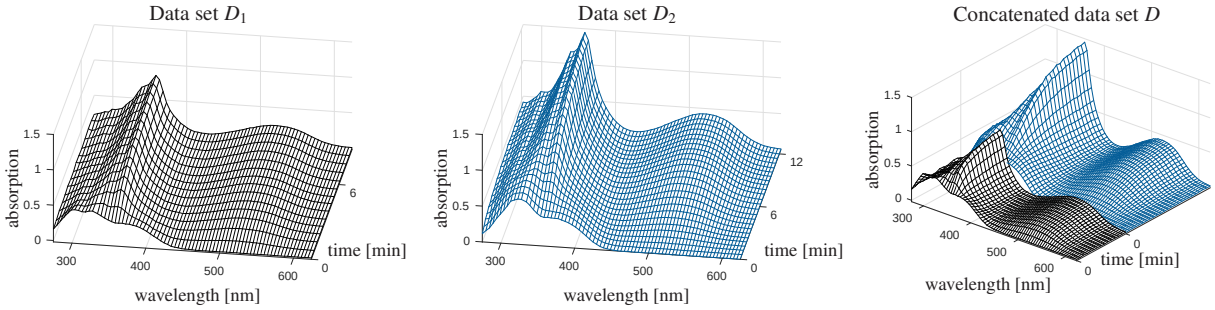

Figure 1: On the left the data set D_1 and in the middle the data set D_2 are shown. The matrix D is the result of merging the data sets D_1 and D_2 as in Equation (2) and is presented in the right plot.

Before applying the hard-modeling approach from Section 2, approximations of the photokinetic factors $F_1(t)$ and $F_2(t)$ have to be determined for D_1 and D_2. The 269$^{\text{th}}$ component of x reads 404.98nm and is nearest to the value of the irradiation wavelength $\lambda = 405$nm. The evaluation of (14) is done for the time discrete intensity profiles $D_1(:, 269), D_2(:, 269)$ and reads $\bar{F}_1 \in \mathbb{R}^{103}$ and $\bar{F}_2 \in \mathbb{R}^{146}$. Additionally, a Savitzky-Golay filter with 3$^{\text{rd}}$ degree polynomials and a window width of 35 points has proven to be suitable in order to reduce the influence of noise. The resulting vectors are called $\bar{F}_1^s \in \mathbb{R}^{103}$ and $\bar{F}_2^s \in \mathbb{R}^{146}$. Fig. 2 shows the raw and smoothed approximations of the photokinetic factors.

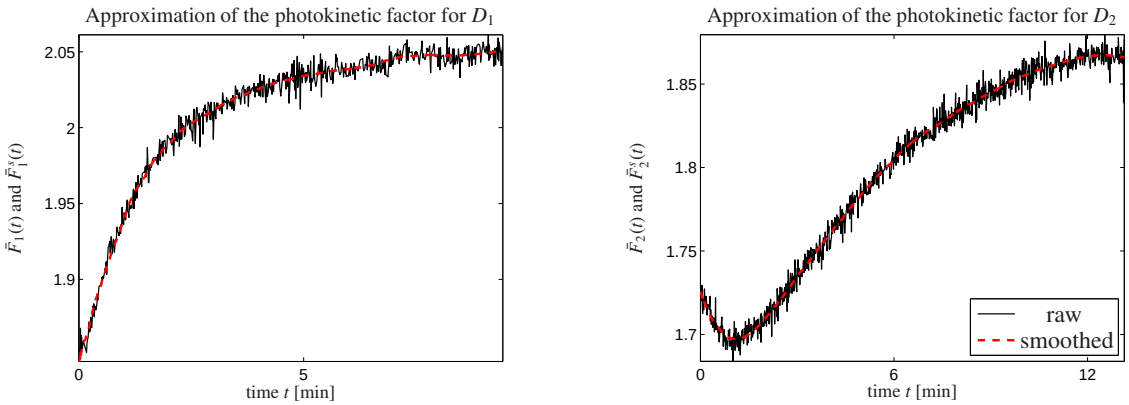

Figure 2: The approximations $\bar{F}_1$ and $\bar{F}_2$ of the photokinetic factors determined by Equation (14) are plotted in black. The smoothed approximations $\bar{F}_1^s$ and $\bar{F}_2^s$ were obtained by a Savitzky-Golay filter and are shown as red dashed lines.

Next, the hard-modeling approach from Section 2 is used to calculate a decomposition which is consistent with the given photokinetic model (5). A solution to the minimization problem (4) is computed with the solver *lsqnonlin* from MatLab 2017b. The calculated quantum yields are $\phi^* = (0.1429, 0.2491, 0.2219, 0.3678)^T$ and the corresponding factors C^* and S^* are shown in Fig. 3. The obtained relative errors are

$$\frac{\|D - C^*(S^*)^T\|_F}{\|D\|_F} = 0.010, \quad \frac{\|C^* - C^{\text{ode}}(\phi^*)\|_F}{\|C^*\|_F} = 0.022, \quad \frac{\|\min(C^*, 0)\|_F}{\|C^*\|_F} = 0.0012, \quad \frac{\|\min(S^*, 0)\|_F}{\|S^*\|_F} = 0.00052.$$

Because of the noisy/perturbed spectral data these error values do not exactly equal 0. Therefore the sets $\mathcal{K}$ and $\mathcal{K}_+$ also contain quantum yields for which the corresponding factors have comparably small relative errors.

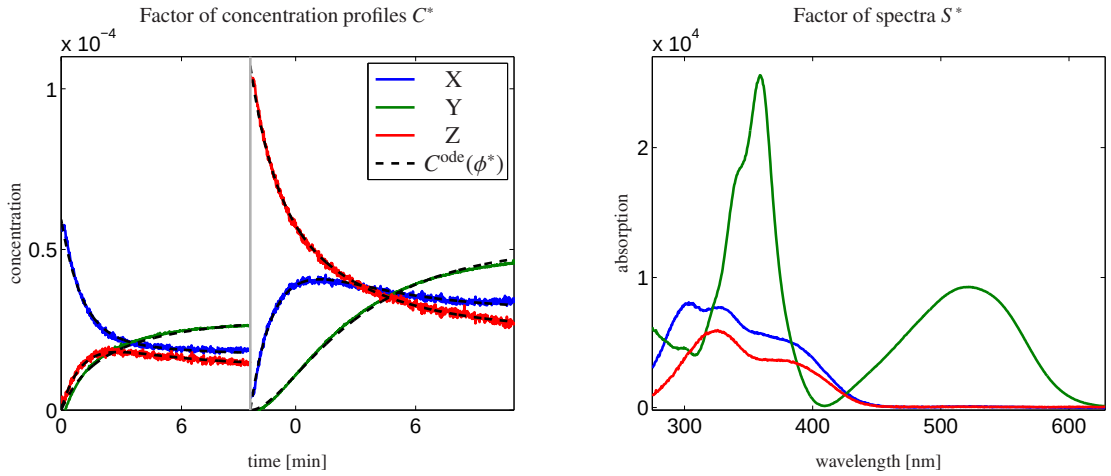

Figure 3: Decomposition of the merged matrix D from Fig. 1; On the left the concentration profiles C^* are shown in color together with the kinetic model $C^{\mathrm{ode}}(\phi^*)$ as black dashed lines. The corresponding spectral profiles S^* are shown on the right. They are valid for both data sets D_1 and D_2.

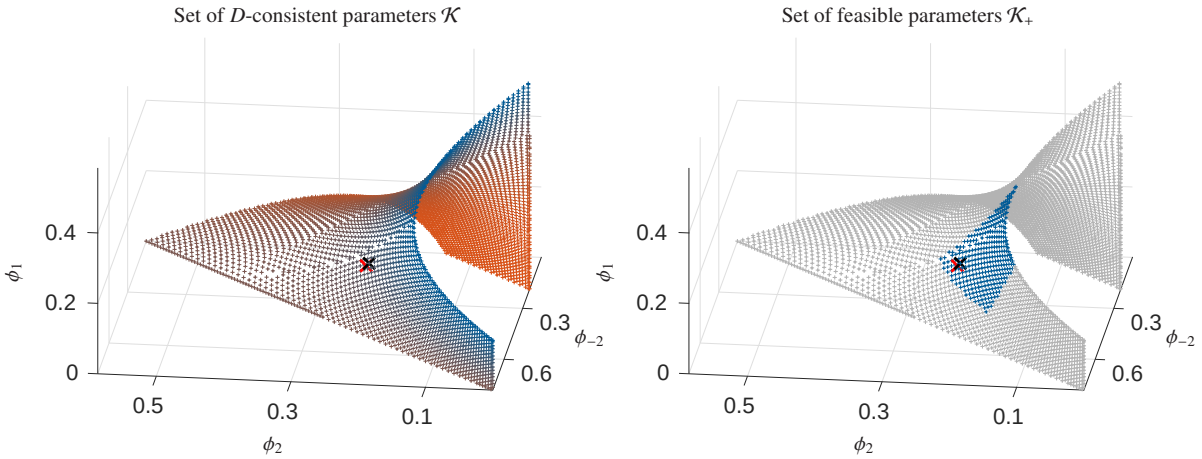

Figure 4: Representation of the sets $\mathcal{K}$ (left) and $\mathcal{K}_+$ (right); The set of representatives of $\mathcal{K}$ is shown as colored points in the left plot and is obtained by the use of the Equations (10)-(13). Because of noisy data the nonnegativity constraint of the factor S for $\mathcal{K}_+$ has been applied with a tolerance of 2%. This results in the blue colored subset $\mathcal{K}_+$ of $\mathcal{K}$ in the right plot. The quantum yields ϕ^* are marked by a black cross and ϕ^{opt} by a red cross in each plot.

Next the analytical description of the set $\mathcal{K}$ for the photokinetic model (5) from Section 3 is used. The initial values $\kappa(\phi^*) = 2263.51$ and $\delta(\phi^*) = 800718.27$ are first computed. Thus the eigenvalues of $M(\phi^*)$ are $\lambda_1 = 0, \lambda_2 = -438.83$ and $\lambda_3 = -1824.68$. An evaluation of $\phi_1(\phi_2, \phi_{-2})$ from Equation (12) is done for values in the (ϕ_2, ϕ_{-2})-plane. Only those values have to be considered for which the constraints from Equation (10) and (11) hold. The corresponding values for $\phi_{-1}(\phi_2, \phi_{-2})$ are given by Equation (13). They can be neglected in order to reduce the dimension which is needed to display $\mathcal{K}$. The left plot of Fig. 4 shows an approximation of the set $\mathcal{K}$ by a set of representatives. The quantum yield vector $\phi^* \in \mathcal{K}$ is used to compute κ, δ and thus also $\mathcal{K}$. It is marked by a black cross.

The second step is a reduction of $\mathcal{K}$ to $\mathcal{K}_+$. To this end the factor S is calculated for each representative of $\mathcal{K}$ in a way that the objective function (3) is minimized. If

$$|\min(S(i,:),0)| \leq 0.02 \cdot \max(S(i,:)) \tag{15}$$

holds, then the scaled factor S (in way that all columns have a maximum of 1) contains no entry below -0.02. In other words, this strategy amounts to the acceptance of 2% negative entries in S. In conclusion the corresponding representative in $\mathcal{K}$ also belongs to $\mathcal{K}_+$, if (15) holds for $i = 1, \ldots, s$. The result is shown in blue color in the right plot of Fig. 4. Both sets $\mathcal{K}$ and $\mathcal{K}_+$ are consistent with the approximations calculated using the grid search algorithm in

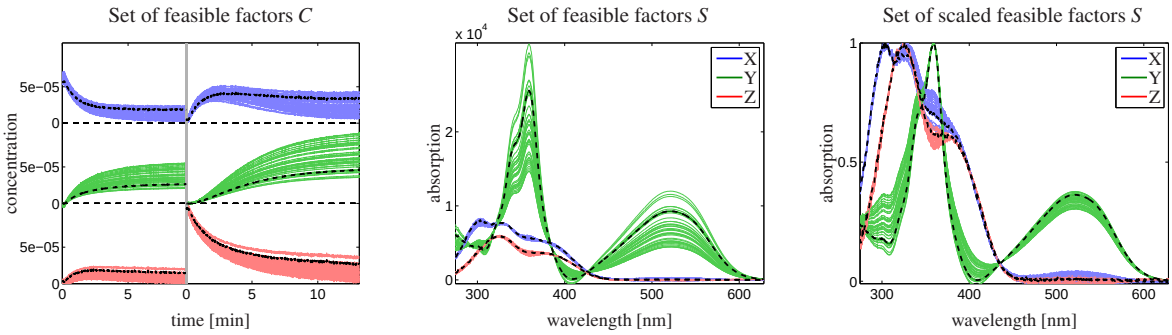

Figure 5: The factors C (left) and S (center) are shown for each representative of $\mathcal{K}_+$ in Fig. 4. Qualitative and quantitative differences can be observed for all species. The two plots can be interpreted as representation of the rotational ambiguity constrained by a kinetic model. A scaling to a maximal height of 1 for each spectrum is used in the right plot. This highlights that most of the feasible factors S contain a similar structural information. Nevertheless the corresponding factors C show major differences. It should be noted that not only bands of solutions are shown, but a set of individual feasible factors. To emphasize this the factors C_{opt} and S_{opt} for ϕ_{opt} are plotted by black dashed lines.

[27]. The associated bands corresponding to these feasible factors C and S are plotted in Fig. 5. These plots constitute graphical evaluations of the rotational ambiguity of a data set under the constraint of a kinetic model. In the left and the center plot we use a scaling that is determined by the kinetic model. Consequently, scalar multiples of the same concentration profile or spectrum also appear in the plots. For better graphical evaluation of the rotational ambiguity a max-height-of-1 scaling is used in the right plot.

Next, the correctness of the set $\mathcal{K}_+$ is validated. Therefore, the nonnegativity and the fit to the kinetic model is evaluated for all the representatives of $\mathcal{K}_+$ as plotted in Fig. 4. Table 1 contains the relative errors for ϕ^* as reference values as well as the corresponding lower and upper bounds. The relative error is between 0.0009 and 0.015 for the

	$\|C - C^{\text{ode}}(\phi)\|_F / \|C\|_F$	$\|\min(C,0)\|_F / \|C\|_F$	$\|\min(S,0)\|_F / \|S\|_F$
$\phi = \phi^*$	0.022	1.2 E−3	5.2 E−4
Upper bound for all $\phi \in \mathcal{K}_+$	0.067	1.5 E−2	9.8 E−3
Lower bound for all $\phi \in \mathcal{K}_+$	0.020	9.0 E−4	4.0 E−4
$\phi = \phi^{\text{opt}}$	0.021	1.1 E−3	5.1 E−4

Table 1: The relative errors of the corresponding factors for the vector of quantum yields ϕ^* and ϕ^{opt} as well as lower and upper bounds are listed.

nonnegativity of C and between 0.0004 and 0.0098 for the nonnegativity of S. This is considered to be sufficiently good. The relative error for the kinetic fit ranges between 0.02 and 0.067. The relatively large upper limit is caused by the noise contained in D_1 and D_2, which is mainly found in the concentration factors (compare the left and right plot in Fig. 3).

In the final step of the analysis the representatives of the set $\mathcal{K}$ are scanned for a vector of quantum yields which results in smaller error values compared to that which belong to ϕ^*. The optimal vector of quantum yields reads $\phi^{\text{opt}} = (0.1355, 0.2592, 0.2263, 0.3671)$. Its relative error values are listed in the last row of Table 1. Optimality is to be understood in the sense of smallest error values. This does not necessarily include that the found solution has the greatest chemical meaning. Nevertheless, these two interpretations are often correlated. The optimal vector is marked by a red cross in Fig. 4. The two vectors ϕ^* and ϕ^{opt} differ only slightly. A graphical comparison of corresponding factors $C_{\text{opt}}, S_{\text{opt}}$ (colored) with C^*, S^* (gray) is given in Fig. 6. While the spectra of the components X and Z remain nearly unchanged, a clear difference can be seen for the spectrum of the second component Y. Additionally, the concentration profiles show major differences in all components. Hence the small difference between ϕ^* and ϕ^{opt} can yield qualitatively different but still feasible solutions.

5. Conclusion

Kinetic models can support MCR methods in reducing the rotational ambiguity of pure component factorizations for bilinear data. However, even under the constraint of the consistence to a kinetic hard model, a unique factorization

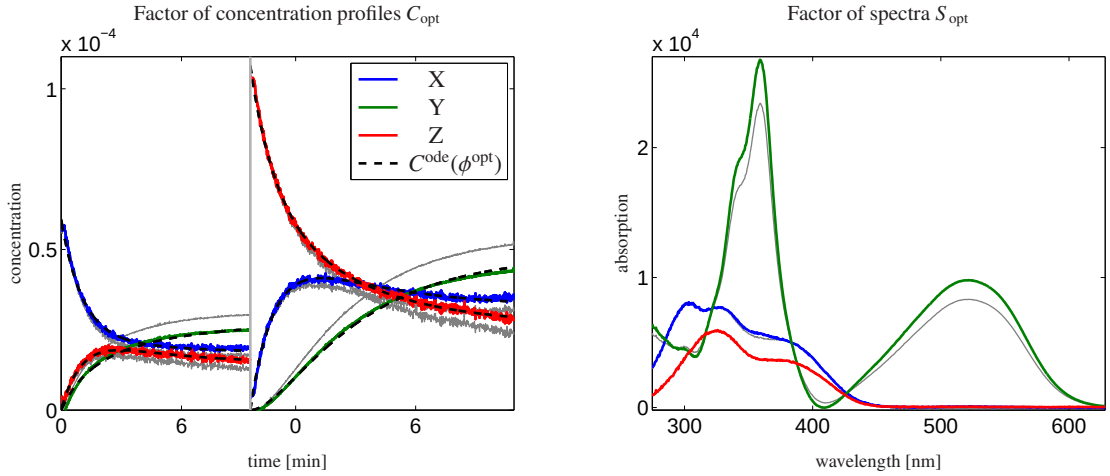

Figure 6: Decomposition of the merged matrix D from Fig. 1; On the left the concentration profiles C^{opt} are shown in color together with the kinetic model solution $C^{ode}(\phi^{opt})$ by black dashed lines. The corresponding spectral profiles S^{opt} are shown on the right. The factors C^* and S^* are also plotted in gray for comparison purposes.

cannot always be guarantied.

In this paper we have demonstrated a mathematical analysis which allows us to investigate the remaining ambiguity of a kinetic-hard-model based MCR approach. The ambiguity is presented in closed-form mathematical expressions for the quantum yield vectors of a reversible two-step photochemical system that are consistent with the spectroscopic data.

We hope that the presented strategy on the hand can raise awareness for MCR-ambiguities even under the kinetic-hard-model conditions and on the other hand can highlight the strength of the mathematical-analytic representation of the set of feasible quantum yields.

Appendix A. Equations for the analytical description of $\mathcal{K}$

This section contains the mathematical derivation of the Equations (10)-(13) that describe the set $\mathcal{K}$ for the kinetic model (5). We assume that the two eigenvalues λ_2 and λ_3 in Equation (8) are enumerated in a way that $0 > \lambda_2 > \lambda_3$. The two sets

$$\mathcal{M} := \left\{ \phi \in (0,1]^4 \ : \ \lambda_{2,3} = -\frac{\kappa(\phi)}{2} \pm \frac{1}{2}\sqrt{\kappa(\phi)^2 - 4\delta(\phi)} \right\},$$
$$\mathcal{N} := \left\{ \phi \in (0,1]^4 \ : \ \text{Eq. (10)-(13) hold} \right\}$$

are to be considered with $\kappa(\phi)$ and $\delta(\phi)$ by (9). It has to be shown that $\mathcal{M} = \mathcal{N}$ or equivalently that $\phi \in \mathcal{M}$ if and only if $\phi \in \mathcal{N}$.

First we prove that $\phi \in \mathcal{M}$ implies that $\phi \in \mathcal{N}$. In a preparation step we show that the following term equals 0:

$$\begin{aligned}
&(\varepsilon_X\phi_2 + \varepsilon_Z\phi_{-2})^2 - (\varepsilon_X\phi_1 + \varepsilon_X\phi_2 + \varepsilon_Z\phi_{-2})(\varepsilon_X\phi_2 + \varepsilon_Z\phi_{-2}) + \varepsilon_X\phi_1\varepsilon_Z\phi_{-2} + \varepsilon_X\phi_1\varepsilon_X\phi_2 \qquad \text{(A.1)}\\
&= (\varepsilon_X\phi_2 + \varepsilon_Z\phi_{-2})^2 - (\underbrace{\varepsilon_X\phi_1 - \varepsilon_X\phi_1}_{=0} + \varepsilon_X\phi_2 + \varepsilon_Z\phi_{-2})(\varepsilon_X\phi_2 + \varepsilon_Z\phi_{-2})\\
&= (\varepsilon_X\phi_2 + \varepsilon_Z\phi_{-2})^2 - (\varepsilon_X\phi_2 + \varepsilon_Z\phi_{-2})^2\\
&= 0\,.
\end{aligned}$$

Next we subtract the term $\varepsilon_X\phi_1\varepsilon_X\phi_2$ from (A.1) and divide the equation by $\varepsilon_X^2\phi_2$. This results in

$$\begin{aligned}
\phi_1(\phi_2,\phi_{-2}) &= -\frac{1}{\varepsilon_X^2\phi_2}\cdot((\varepsilon_X\phi_2+\varepsilon_Z\phi_{-2})^2-(\varepsilon_X\phi_1+\varepsilon_X\phi_2+\varepsilon_Z\phi_{-2})(\varepsilon_X\phi_2+\varepsilon_Z\phi_{-2})+\varepsilon_X\phi_1\varepsilon_Z\phi_{-2})\\
&= -\frac{1}{\varepsilon_X^2\phi_2}\cdot((\varepsilon_X\phi_2+\varepsilon_Z\phi_{-2})^2-(\varepsilon_X\phi_1+\underbrace{\varepsilon_X\phi_{-1}-\varepsilon_X\phi_{-1}}_{=0}+\varepsilon_X\phi_2+\varepsilon_Z\phi_{-2})(\varepsilon_X\phi_2+\varepsilon_Z\phi_{-2})+\varepsilon_X\phi_1\varepsilon_Z\phi_{-2})\\
&= -\frac{1}{\varepsilon_X^2\phi_2}\cdot((\varepsilon_X\phi_2+\varepsilon_Z\phi_{-2})^2-\underbrace{\kappa(\phi)}_{=-(\lambda_2+\lambda_3)}(\varepsilon_X\phi_2+\varepsilon_Z\phi_{-2})+\underbrace{\delta(\phi))}_{=\lambda_2\lambda_3}\\
&= -\frac{1}{\varepsilon_X^2\phi_2}\cdot((\varepsilon_X\phi_2+\varepsilon_Z\phi_{-2})^2+(\varepsilon_X\phi_2+\varepsilon_Z\phi_{-2})(\lambda_2+\lambda_3)+\lambda_2\lambda_3)\\
&= -\frac{1}{\varepsilon_X^2\phi_2}\cdot(\varepsilon_X\phi_2+\varepsilon_Z\phi_{-2}+\lambda_2)\cdot(\varepsilon_X\phi_2+\varepsilon_Z\phi_{-2}+\lambda_3)\,.
\end{aligned}$$

This shows that Equation (12) holds. Equation (13) follows directly from the fact that $\kappa(\phi)=-(\lambda_2+\lambda_3)$ is constant for all $\phi\in\mathcal{M}$ so that $\kappa(\phi)=\kappa(\phi^*)$.

The nonnegativity of $\phi_1(\phi_2,\phi_{-2})$ and the representation by Equation (12) imply that

$$(\varepsilon_X\phi_2+\varepsilon_Z\phi_{-2}+\lambda_2)\cdot(\varepsilon_X\phi_2+\varepsilon_Z\phi_{-2}+\lambda_3)<0\,.$$

Due to $\lambda_3<\lambda_2<0$ the latter inequality can only hold if $\varepsilon_X\phi_2+\varepsilon_Z\phi_{-2}+\lambda_2$ is positive and $\varepsilon_X\phi_2+\varepsilon_Z\phi_{-2}+\lambda_3$ is negative. This proves (10).

Next the equation

$$(\varepsilon_Z\phi_{-2}+\lambda_2)(\varepsilon_Z\phi_{-2}+\lambda_3)=(\varepsilon_Z\phi_{-2})^2+\varepsilon_Z\phi_{-2}(\underbrace{\lambda_2+\lambda_3}_{-\kappa})+\underbrace{\lambda_2\lambda_3}_{\delta}=\varepsilon_X\phi_2\varepsilon_Z\phi_{-2}+\varepsilon_X\phi_2\varepsilon_Y\phi_{-1}=\varepsilon_X\phi_2(\varepsilon_Z\phi_{-2}+\varepsilon_Y\phi_{-1})$$

holds and hence we get

$$\phi_2>0>\underbrace{-\frac{\varepsilon_X\phi_2}{\varepsilon_X\varepsilon_Z\phi_{-2}}(\varepsilon_Z\phi_{-2}+\varepsilon_Y\phi_{-1})}_{>0}=-\frac{1}{\varepsilon_X\varepsilon_Z\phi_{-2}}(\varepsilon_Z\phi_{-2}+\lambda_2)(\varepsilon_Z\phi_{-2}+\lambda_3)\,.$$

Thus (11) holds.

Finally we show the reverse direction, namely that $\phi\in\mathcal{N}$ implies that $\phi\in\mathcal{M}$. We only have to show that $\kappa(\phi)=\kappa(\phi^*)$ and $\delta(\phi)=\delta(\phi^*)$. With (8) this proves that $M(\phi)$ has the same eigenvalues as $M(\phi^*)$ which completes the proof.

First, $\kappa(\phi)=\kappa(\phi^*)$ results from a simple reorganization of Eq. (13). Second, starting from (12) the equation

$$\begin{aligned}
\phi_1(\phi_2,\phi_{-2}) &= -\frac{1}{\varepsilon_X^2\phi_2}\cdot(\varepsilon_X\phi_2+\varepsilon_Z\phi_{-2}+\lambda_2)\cdot(\varepsilon_X\phi_2+\varepsilon_Z\phi_{-2}+\lambda_3)\\
&= -\frac{1}{\varepsilon_X^2\phi_2}\cdot((\varepsilon_X\phi_2+\varepsilon_Z\phi_{-2})^2+(\varepsilon_X\phi_2+\varepsilon_Z\phi_{-2})\underbrace{(\lambda_2+\lambda_3)}_{-\kappa(\phi^*)}+\underbrace{\lambda_2\lambda_3)}_{\delta(\phi^*)}\\
&= -\frac{1}{\varepsilon_X^2\phi_2}\cdot((\varepsilon_X\phi_2+\varepsilon_Z\phi_{-2})^2-\kappa(\phi)(\varepsilon_X\phi_2+\varepsilon_Z\phi_{-2})+\delta(\phi^*))
\end{aligned}$$

follows. Multiplication by $\varepsilon_X^2\phi_2$ and subtraction of $\varepsilon_X^2\phi_2\phi_1(\phi_2,\phi_{-2})$ gives

$$0=-((\varepsilon_X\phi_2+\varepsilon_Z\phi_{-2})^2-\kappa(\phi)(\varepsilon_X\phi_2+\varepsilon_Z\phi_{-2})+\delta(\phi^*))-\varepsilon_X^2\phi_2\phi_1(\phi_2,\phi_{-2}).\tag{A.2}$$

Expansion of the quadratic term and substitution of $\kappa(\phi)$ by its definition reduces (A.2) to

$$0=\varepsilon_X\phi_1\varepsilon_Z\phi_{-2}+\varepsilon_Y\phi_{-1}\varepsilon_X\phi_2+\varepsilon_Y\phi_{-1}\varepsilon_Z\phi_{-2}-\delta(\phi^*))=\delta(\phi)-\delta(\phi^*).$$

Hence $\delta(\phi)=\delta(\phi^*)$ has been proved.

References

[1] E. Malinowski. *Factor analysis in chemistry*. Wiley, New York, 2002.

[2] M. Maeder and Y.M. Neuhold. *Practical data analysis in chemistry*. Elsevier, Amsterdam, 2007.

[3] H. Abdollahi and R. Tauler. Uniqueness and rotation ambiguities in multivariate curve resolution methods. *Chemom. Intell. Lab. Syst.*, 108(2):100–111, 2011.

[4] J. Jaumot, R. Gargallo, A. de Juan, and R. Tauler. A graphical user-friendly interface for MCR-ALS: a new tool for multivariate curve resolution in MATLAB. *Chemom. Intell. Lab. Syst.*, 76(1):101–110, 2005.

[5] H. Kim and H. Park. Nonnegative matrix factorization based on alternating nonnegativity constrained least squares and active set method. *SIAM J. Matrix Anal. Appl.*, 30:713–730, 2008.

[6] J. Jaumot, A. de Juan, and R. Tauler. MCR-ALS GUI 2.0: new features and applications. *Chemom. Intell. Lab. Syst.*, 140:1–12, 2015.

[7] R. Tauler. Calculation of maximum and minimum band boundaries of feasible solutions for species profiles obtained by multivariate curve resolution. *J. Chemom.*, 15(8):627–646, 2001.

[8] O.S. Borgen and B.R. Kowalski. An extension of the multivariate component-resolution method to three components. *Anal. Chim. Acta*, 174:1–26, 1985.

[9] R. Rajkó and K. István. Analytical solution for determining feasible regions of self-modeling curve resolution (SMCR) method based on computational geometry. *J. Chemom.*, 19(8):448–463, 2005.

[10] M. Sawall, C. Kubis, D. Selent, A. Börner, and K. Neymeyr. A fast polygon inflation algorithm to compute the area of feasible solutions for three-component systems. I: Concepts and applications. *J. Chemom.*, 27:106–116, 2013.

[11] A. Jürß, M. Sawall, and K. Neymeyr. On generalized Borgen plots. I: From convex to affine combinations and applications to spectral data. *J. Chemom.*, 29(7):420–433, 2015.

[12] A. de Juan, M. Maeder, M. Martínez, and R. Tauler. Combining hard and soft-modelling to solve kinetic problems. *Chemom. Intell. Lab. Syst.*, 54:123–141, 2000.

[13] M. Sawall, A. Börner, C. Kubis, D. Selent, R. Ludwig, and K. Neymeyr. Model-free multivariate curve resolution combined with model-based kinetics: Algorithm and applications. *J. Chemom.*, 26:538–548, 2012.

[14] N. Mouton, A. de Juan, M. Sliwa, and C. Ruckebusch. Hybrid hard- and soft-modeling approach for the resolution of convoluted femtosecond spectrokinetic data. *Chemom. Intell. Lab. Syst.*, 105(1):74 – 82, 2011.

[15] H. Schröder, M. Sawall, C. Kubis, D. Jürß, A. Selent, A. Brächer, A. Börner, R. Franke, and K. Neymeyr. Comparative multivariate curve resolution study in the area of feasible solutions. *Chemom. Intell. Lab. Syst.*, 163:55–63, 2017.

[16] N.W. Alcock, D.J. Benton, and P. Moore. Kinetics of Series First-Order Reactions. *Trans. Faraday Soc.*, 66:2210–2213, 1970.

[17] S. Vajda and H. Rabitz. Identifiability and distinguishability of first-order reaction systems. *J. Phys. Chem.*, 92(3):701–707, 1988.

[18] J. Jaumot, P. J. Gemperline, and A. Stang. Non-negativity constraints for elimination of multiple solutions in fitting of multivariate kinetic models to spectroscopic data. *J. Chemom.*, 19(2):97–106, 2005.

[19] H. Schröder, M. Sawall, C. Kubis, D. Selent, D. Hess, R. Franke, A. Börner, and K. Neymeyr. On the ambiguity of the reaction rate constants in multivariate curve resolution for reversible first-order reaction systems. *Anal. Chim. Acta*, 927:21–34, 2016.

[20] R. Tauler, A. Smilde, and B. Kowalski. Selectivity, local rank, three-way data analysis and ambiguity in multivariate curve resolution. *Journal Chemom.*, 9(1):31–58, 1995.

[21] L. Blanchet, C. Ruckebusch, A. Mezzetti, J. P. Huvenne, and A. de Juan. Monitoring and interpretation of photoinduced biochemical processes by rapid-scan ftir difference spectroscopy and hybrid hard and soft modeling. *J. Phys. Chem. B*, 113(17):6031–6040, 2009. PMID: 19385692.

[22] O. Devos, S. Aloise, M. Sliwa, R. Métivier, J.-P. Placial, and C. Ruckebusch. Chapter 11 - multivariate curve resolution of (ultra)fast photoinduced process spectroscopy data. In Cyril Ruckebusch, editor, *Resolving Spectral Mixtures*, volume 30 of *Data Handling in Science and Technology*, pages 353 – 379. Elsevier, 2016.

[23] G.H. Golub and C.F. Van Loan. *Matrix Computations*. Johns Hopkins Studies in the Mathematical Sciences. Johns Hopkins University Press, Baltimore, MD, 2012.

[24] J. C. Lagarias, J. A. Reeds, M. H. Wright, and P. E. Wright. Convergence properties of the nelder-mead simplex method in low dimensions. *SIAM J. Optim.*, 9(1):112–147, 1998.

[25] T. F. Coleman and Y. Li. An interior trust region approach for nonlinear minimization subject to bounds. *SIAM J. Optim.*, 6(2):418–445, 1996.

[26] H. Mauser and G. Gauglitz. *Photokinetics: theoretical fundamentals and applications*, volume 36. Elsevier, 1998.

[27] O. Devos, H. Schröder, M. Sliwa, J.P. Placial, K. Neymeyr, R. Metivier, and C. Ruckebusch. Photochemical multivariate curve resolution models for the investigation of photochromic systems under continuous irradiation. *Accepted by Anal. Chim. Acta*, 2018.